Ion composition of expanding microdischarges in dielectric barrier discharges

Xudong Peter Xu[a] and Mark J. Kushner[b]
Department of Electrical and Computer Engineering, University of Illinois, 1406 W. Green Street, Urbana, Illinois 61801

(Received 13 November 1997; accepted for publication 10 March 1998)

The properties of the filamentary microdischarges found in dielectric barrier discharges depend on the manner of charging of the dielectric. The charging of the dielectric removes voltage from the gap thereby reducing E/N and producing a transition from an avalanching discharge to a recombination or attachment dominated discharge. In this article, we report on a computational investigation of these processes using a one-dimensional plasma chemistry model. We find that the expansion and ultimate stalling of the microdischarge is largely determined by charging of the dielectric at larger radii than the core of the microdischarge. The lowering of E/N in the core of the microdischarge in attaching gases can quickly consume electrons. This transition produces a discharge consisting of an expanding shell having a high electron density and an inner core dominated by negative ions. In extreme cases where the gas mixture contains thermal electron attaching gases, the core of the microdischarge is essentially a negative ion-positive ion plasma. Using square wave voltage pulses, the residual charge on the dielectric after the microdischarge, which contributes to the gap voltage on the next voltage pulse, is largely determined by the attachment rate in the core of the microdischarge. Rapid attachment reduces the plasma conductivity and leaves residual charge on the dielectric. © *1998 American Institute of Physics.* [S0021-8979(98)00212-6]

I. INTRODUCTION

Dielectric barrier discharges (DBDs), or silent electrical discharges, have long been used for ozone syntheses,[1–3] and are now being investigated for use in plasma remediation of toxic gases. DBDs have been applied to remediation of SO_2 and oxides of nitrogen (N_xO_y) from combustion of fossil fuels,[4–7] and to treat volatile organic compounds (VOCs).[8–13] By applying an alternating (sine or square wave) potential of several to 10 kV with a frequency of a few hundreds to several kHz to the electrodes, at least one of which is covered by a dielectric, filamentary microdischarges are created having area densities of 10–100 s cm^{-2}. These microdischarges are statistically spread evenly throughout the discharge. The discharge plasma channels are terminated when charge accumulation on the dielectric surface (or surfaces) reduces the voltage across the gap at the position of the microdischarge to a value below that which is self-sustaining. The gap voltage at other locations, whose dielectric is uncharged and which has not experienced a microdischarge, remain at the line potential. Typical microdischarge current pulses have durations of a few to 100 ns and diameters of 10–100 s μm.

Several investigations have computationally addressed microdischarge dynamics in DBDs. In particular, one-dimensional simulations have been performed in the direction perpendicular to the electrodes.[14] These studies have shown that early during the discharge pulse, the electric field is large in the gap, however, formation of a cathode fall reduces the bulk electric field which in turn reduces excitation rates. These observations emphasize the need for fast rising, short voltage pulses to maximize the efficiency of radical production. Eliasson and Kogelschatz[3] developed a two-dimensional simulation [(r,z) in the plane perpendicular to the electrodes] to investigate the expansion of the microdischarge and charging of the dielectric. The model was applied to xenon microdischarges for excimer lighting sources and oxygen for ozone synthesis. They found that for a 1 mm gap in 1 atm of oxygen, the microdischarge expanded to a radius of 10–100 μm in $\approx$50 ns at which time the expansion terminated. They found that the charge on the surface of the dielectric typically extended to a larger radius than the body of the microdischarge. One interpretation of their results is that lateral spreading of current in the vicinity of the dielectric surface charges the dielectric at larger radii than the core of the microdischarge. As a consequence, the potential and axial electric field is reduced at large radii, which in turn prevents the microdischarge from expanding further. An extreme manifestation of this effect is Lichtenberg figures.[15] Similar computational results were obtained by Braun, Gibalov and Pietsch.[16]

In typical applications of DBDs, the gas pressure is sufficiently large ($pd>75–100$ Torr cm) and current pulses sufficiently short (<10 s ns) that diffusion is not a dominant process in the ion kinetics. Volumetric processes (ionization, attachment and dissociative recombination), which are generally exponentially dependent on the magnitude of the local electric field, preferentially determine the ion density and mole fractions. Typically, there is a unique value of E/N

[a]Electronic mail: xxu@uiuc.edu
[b]Electronic mail: mjk@uiuc.edu

(electric field/gas number density) for a given gas mixture at which a self-sustaining or steady state ion kinetics can be achieved and where volumetric ion sources balance volumetric ion sinks. (This is only strictly true for discharges dominated by attachment and in which multistep processes are not important.) At a given radial location, as the microdischarge charges the dielectric and removes voltage from the gap, the electric field in the bulk plasma necessarily transitions from being above self-sustaining (required to avalanche the gas) to being below self sustaining (required to extinguish the discharge).

The dependence of rate coefficients for ionization, attachment, recombination and ion-ion neutralization on E/N can be markedly different. As a result the ion kinetics, and therefore ion composition, of the microdischarge can be expected to be very different as a function of time as the dielectric charges and E/N changes. This situation is further complicated by the fact that the microdischarge radially expands during the current pulse from 10 to 100 s μm. As the microdischarge expands, the sequence of avalanche, dielectric charging and quenching occurs in a wave-like fashion propagating to larger radii. Ion composition may therefore depend not only on time but also on radius. Since ion chemistry can greatly affect the efficiency of, for example, plasma remediation processes, the radial dynamics of microdischarge expansion and their effect on ion chemistry, warrant further study.

In this article, we apply a one-dimensional radially dependent plasma chemistry model to the study of ion kinetics in an expanding microdischarge in a DBD. The goal of this investigation is to quantify the transition of the bulk E/N from avalanche to below self sustaining as the microdischarge expands, and to determine the consequences of this behavior on charged particle densities. We acknowledge the importance of neutral radicals in plasma remediation, but will not be addressing their dynamics in this paper as our interest here is primarily the cited transition between high E/N to low E/N excitation which, on the time scales of interest, primarily affects the composition of ions.

The context of this study is the use of DBDs for toxic gas remediation which may involve a large variety of gases having very different ion chemistries. In an attempt to span this parameter space, we investigated three representative gas systems: Ar and N_2 (nonattaching); Ar/O_2 and $N_2/O_2/H_2O$ (moderately attaching); and $Ar/O_2/CCl_4$ (highly attaching). In all cases, the ionization rate coefficients have exponential dependencies on E/N. In nitrogen and argon, the dominant channel for electron and ion removal is dissociative recombination whose dependence on E/N is at best weak. In Ar/O_2 and $N_2/O_2/H_2O$, dissociative electron attachment to O_2 and H_2O is resonant, and so the additional electron loss by this mechanism peaks at a nonzero E/N. On the other hand, due to the large thermal attachment cross section for CCl_4, even small amounts of the halogen in $Ar/O_2/CCl_4$ mixtures produces a significant increase in attachment which has a maximum rate at zero E/N. We find that as the E/N in the bulk plasma transitions from avalanche to below self sustaining, the ion kinetics in these three representative systems differ markedly.

A brief description of the model we have used in this work appears in Sec. II followed by a discussion of microdischarge dynamics during expansion in Sec. III. Our concluding remarks are given in Sec. IV.

II. DESCRIPTION OF THE MODEL AND REACTION MECHANISMS

The model used in this study is a modified version of the one-dimensional microdischarge simulation previously discussed in Ref. 17. The model begins by assuming that the DBD is composed of a uniformly spaced array of identical radially symmetric microdischarges. The numerical mesh is discretized in the radial direction with varying resolution from sub-micron near the center of the microdischarge to a few microns at the outer radius. The last numerical cell has a square outer boundary and circular inner boundary in order to apply reflective boundary conditions. The spacing of the microdischarges is sufficiently large that they do not significantly interact, and so a single microdischarge employing reflective boundary conditions can be used. Typically 800–900 radial points are used in the simulation to resolve the problem.

The model is composed of four components: an external circuit model, a solution of Boltzmann's equation for the electron energy distribution, a plasma chemistry model and a transport module. The external circuit model calculates the voltage across the plasma, which is then used to obtain the time evolution of the electron energy distribution from solution of Boltzmann's equation. The heavy particle plasma chemistry model produces the concentrations of neutral and charged particles, and also provides the plasma conductivity for the external circuit model. The motion of species between mesh points is addressed in the transport module. Electron impact rate coefficients for use in the plasma chemistry model are obtained using the local field approximation. Solutions of Boltzmann's equation for the electron energy distribution are parameterized over a wide range of E/N, and the resulting rate and electron impact rate coefficients are placed in a look-up table for use during execution of the model.

The equations we solve in the transport module are:

$$\frac{\partial \rho}{\partial t} = -\nabla \cdot (\rho \mathbf{v}), \tag{1}$$

$$\frac{\partial (\rho \mathbf{v})}{\partial t} = -\nabla P - \nabla \cdot (\rho \mathbf{v}\mathbf{v}) - \nabla \cdot \tau, \tag{2}$$

$$\frac{\partial (c_p \rho T)}{\partial t} = \frac{\partial Q}{\partial t} + \nabla \cdot \kappa \nabla T - \nabla \cdot (c_p \rho T \mathbf{v}) - P(\nabla \cdot \mathbf{v}), \tag{3}$$

where ρ is the mass density, $\mathbf{v}$ is the velocity, T is the temperature, c_p is the heat capacity, P is the thermodynamic pressure (obtained by assuming ideal gas behavior), τ is the viscosity tensor, Q is the enthalpy, and κ is the thermal conductivity. The form of the viscosity tensor we used is given by Thompson.[18] The viscosity and thermal conductivity of the gas were obtained using Lennard Jones parameters and applying the mixture rules as described in Hirschfelder, Curtiss and Bird.[19] The time rate of change in enthalpy is

$$\frac{\partial Q}{\partial t} = \mathbf{J}\cdot\mathbf{E} - \sum_i \left(\frac{dN_i}{dt}\right)\cdot \Delta H_i - \left(\frac{dn_e}{dt}\right)\cdot \frac{3}{2}k\cdot T_e, \qquad (4)$$

where k is Boltzmann's constant, $\mathbf{J}=\sigma\mathrm{E}$, ($\sigma$ is the plasma conductivity) is the current density, $\mathbf{E}$ is the local electric field, H_i is the enthalpy of heavy particle species i having density N_i and T_e is the electron temperature having density n_e. Although the model is 1D in the radial dimension, we account for axial transport by employing no-slip conditions on the top and bottom surfaces, and including the appropriate term in the viscosity tensor.

The densities of individual species are obtained by solving separate continuity equations

$$\frac{\partial \rho_i}{\partial t} = -\nabla\cdot\left[\rho_i\mathbf{v} - \rho D_i \nabla\left(\frac{\rho_i}{\rho}\right)\right] + S_i, \qquad (5)$$

where ρ_i is the mass density of species i, D_i is its diffusion coefficient and S_i is the source function for species i due to electron impact and heavy particle collisions. Ambipolar enhanced diffusion coefficients are used for ions. The transport equations were explicitly integrated in time using a fourth order Runge-Kutta-Gill technique. Spatial derivatives are formulated using conservative finite difference donor cell techniques on a staggered mesh (ρ and T are obtained at cell vertices; $\rho\mathbf{v}$ is obtained at cell boundaries).

In our previous work, a given energy deposition in the microdischarge was specified to enable a quantitative comparison between systems having different operating parameters.[17] In this work, we have utilized parameters more easily identified with the physical device to control energy deposition. These are applied voltage, and dielectric permittivity and thickness. The microdischarge model is one-dimensional in the radial direction and so can at best resolve the discharge and dielectric charging as cylindrical shells and annuli, respectively. In this regard, the discharge circuit is composed of a programmed voltage source, series impedance and the discharge. The discharge is represented by a parallel set of series resistors and capacitors. The resistor accounts for the shell of plasma at a particular mesh point. The capacitor accounts for the annulus of dielectric whose component value is chosen based on the permittivity and thickness of the dielectric. Unless noted otherwise, the line voltage is applied as a square wave. As a result, double periods of electron and radical production are often generated due to charging and discharging the dielectric at the leading and trailing edge of voltage pulse. The pressure is one atmosphere with 0.2 cm gas gap. One electrode is covered by 0.5 mm thickness of a dielectric having permittivity of $5\epsilon_0$.

The species included in each class of discharge ($N_2/O_2/H_2O$, $Ar/O_2/CCl_4$) are listed Table I. (A complete listing of reactions included for each case can be obtained by request from the authors.) These lists are not inclusive of all species which might be encountered in humid air plasmas. A reduced list of species and reactions was formulated to make a more tractable computational problem. In all cases, the dominant source of positive ions is electron impact on ground state species, and feedstock gases in particular. In nonattaching gases the formation of molecular positive ions is followed by dissociative recombination. Addition of O_2 to N_2, or O_2 to Ar, produces additional electron losses by dissociative and three-body electron attachment to O_2, followed by ion-ion recombination between O^- and O_2^- all positive ions. Humid air mixtures add dissociative attachment to H_2O as an electron loss mechanism, followed by ion-ion recombination of H^- with all positive ions. The dissociative attachment cross sections for O_2 and H_2O are similar in that they are resonant and have a threshold energy of 5.38 and 5.53 eV, respectively. In a humid air mixture ($N_2/O_2/H_2O = 79.5/20/0.5$) the dissociative attachment rate coefficient for O_2 exceeds 10^{-11} cm^3/s at E/N$\approx$100 Td and exceeds 10^{-11} cm^3/s for H_2O at E/N$\approx$60 Td). In $Ar/O_2/CCl_4$ mixtures dissociative electron attachment to CCl_4 for even small additions of CCl_4 results in significant increases in electron loss due to the thermal character of the cross section. For example, the rate coefficient for $e+CCl_4\rightarrow CCl_3+Cl^-$ is $4\times10^{-8}-2\times10^{-7}$ cm^{-3} s^{-1} for electron temperatures of 0.1–1 eV.

TABLE I. Main species included in the model.

Gas mixture	Charged species	Neutrals
$N_2/O_2/H_2O$	e, N_2^+, N^+, O_2^+, O^+, O_2^-, O^- H_2O^+, H^-	N_2, $N_2(v)$, $N_2(A)$, N, N(^2D), O_2, $O_2(v)$, $O_2(^1\Delta)$, O_3, O, O(^1D), H_2O, H_2O_2, HO_2, OH, H
$Ar/O_2/CCl_4$	e, Ar^+, Ar_2^+, O_2^+, O^+, O_2^-, O^-, CCl_3^+, CCl_2^+, CCl^+, Cl_2^+, Cl^+, Cl^-	Ar, Ar($4s$), Ar($4p$), Ar_2^*, O_2, $O_2(v)$, $O_2(^1\Delta)$, O_3, O, O(^1D), (CCl_n, $n=1$, 4), Cl_2, Cl, ClO, ClO_2, CCl_3O, CCl_3O_2, CO, CO_2, $COCl_2$

III. MICRODISCHARGE DYNAMICS IN DBDS

We begin our discussion of microdischarge dynamics in DBDs by examining a single microdischarge in pure N_2. The applied voltage is a square pulse of 12 kV magnitude and 40 ns duration. The initial gas pressure is 1 atm at 400 K. The initial seed electron density has a distribution 20 μm in radius and 10^9 cm^{-3} peak value. We have purposely chosen conditions where the microdischarge channel continues to expand as long as there is voltage applied in order to more definitively investigate the effects of dielectric charging on ion chemistry. The consequences of this choice of conditions will be discussed below.

The electron (essentially equal to the N_2^+ density), N atom density and voltage across the gap during and following the voltage pulse are shown in Fig. 1. During the 40 ns that the voltage pulse is on, avalanche in the core of the microdischarge ramps the electron density to a maximum of 1.8×10^{13} cm^{-3}. As the axial discharge current charges the dielectric, voltage is removed from the gap. The dielectric charging time is $\approx$10 ns. After this time, voltage is nearly completely removed from the gap at a given radial location which then terminates the electron avalanche. The microdischarge radius expands by lateral diffusion of electrons to larger radii where the dielectric is uncharged and the electric field is large. Avalanche occurs at the larger radius, which

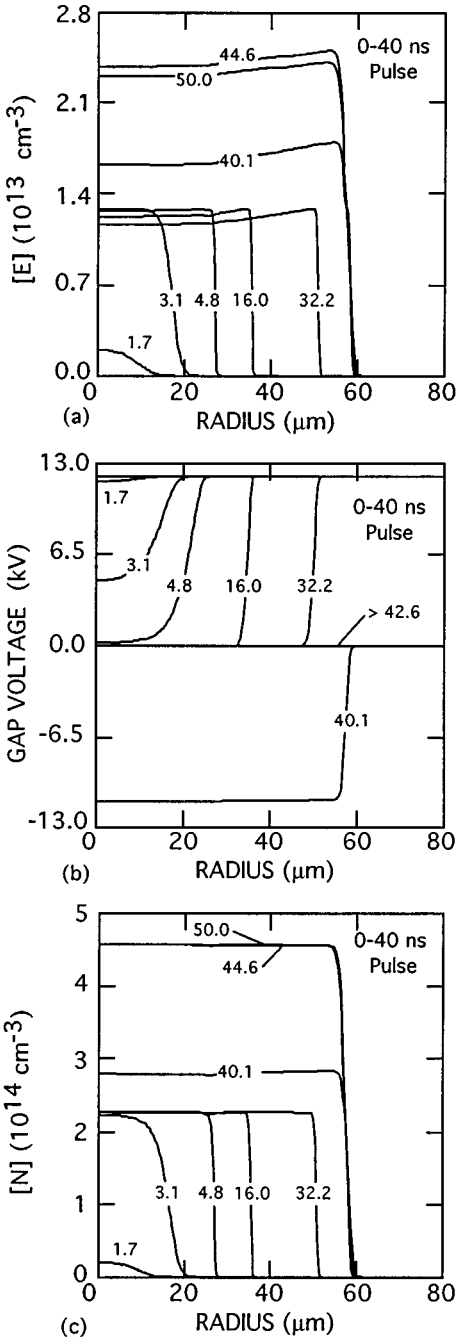

FIG. 1. Microdischarge parameters for a pure N_2 plasma. (a) Electron density, (b) gap voltage and (c) N atom density. The rate of recombination in the core of the streamer is sufficiently low, and conductivity remains sufficiently high, that the dielectric fully charges during the voltage pulse. As a consequence, a secondary avalanche is produced when the line voltage is pulled to zero. The plots for particle densities show values for 0–50 ns as a function of radius at various times. The curves are labeled with their time after application of voltage (ns).

increases the axial current density and charges the dielectric, thereby removing voltage from the gap at that larger radius. As a result, a low voltage region is produced in the core of the microdischarge which propagates outwards, as shown in Fig. 1(b). Since electron-ion recombination is relatively slow (rate coefficient 5×10^{-7} cm^3 s^{-1} yielding a rate of $\approx5\times10^6$ s^{-1}), the electron density decreases by only $\approx10-15\%$ in the core of the microdischarge after the avalanche is terminated by charging of the dielectric, as shown in Fig. 1(a). The end result is a nearly top-hat shaped ion density expanding laterally with a depression in the center due to electron-ion recombination.

Just prior to the end of the 40 ns voltage pulse the dielectric is nearly fully charged to the line voltage. At the end of the voltage pulse, the line voltage is pulled to zero. At this time there is an inverse (or negative) bias across the gap resulting from the previous charging of the dielectric. This inverse voltage extends only to the edge of the just terminated microdischarge. Since the gap is, in a sense, ''preionized'' by the yet to fully recombine plasma, there is a secondary rapid avalanche which nearly doubles the peak ion density. Since the electron density in the microdischarge is large compared to the initial density prior to the primary avalanche, the discharging of the dielectric is more rapid (≈2.6 ns) than the charging and occurs nearly simultaneously across the entire radius. Any lateral diffusion of electrons, of which there is a small component, does not significantly expand the microdischarge. The ''stationary'' microdischarge results from the fact that for the secondary avalanche, the gap voltage beyond the boundary of the microdischarge is zero whereas for the primary avalanche, the gap voltage is always largest outside the microdischarge. After the short secondary avalanche, the electron and ion density continue their slow decrease by dissociative recombination.

The N atom density resembles the ion density as a function of position and time. N atoms, produced by electron impact dissociation of N_2, accumulate during the current pulse since the rate of reassociation to form N_2 (or ionization to form N^+) is slow. The radial profile of the N atom density is even more uniform than that for N_2^+ since the volumetric sink terms and rate of radial diffusion are both smaller for the neutral radical.

The peak gas temperature in the microdischarge depends on the total energy deposition, manner of dissipation of the deposited energy and change in enthalpy due to chemical reactions and radiative decay of excited states. For our default conditions ($\epsilon/\epsilon_0=5$, dielectric capacitance of 88.5 pF/cm^2, 2 mm gas gap, 40 ns 12 kV pulse) the rise in bulk temperature is ≈4 K. The rise is ≈27 K for a line voltage of 17 kV with dielectric capacitance 440 pF/cm^2. As excited states of N_2 are quenched and dissipate their energy into translational modes, there is an additional temperature rise of ≈23 K in the first 0.34 μs after the termination of the voltage pulse. We note that when using high permittivity dielectrics ($50-200\epsilon_0$), there can be sufficiently large temperature rises to induce hydrodynamic effects such as rarefaction.[17]

It was found that for a given line voltage the energy deposition and peak electron density in the microdischarge increased nearly linearly with increasing the dielectric capacitance (either by increasing ϵ or decreasing thickness). The maximum microdischarge radius, however, is a weak function of dielectric properties and energy deposition provided that the line voltage is constant. We found that the rate of expansion of the microdischarge radius depends most sen-

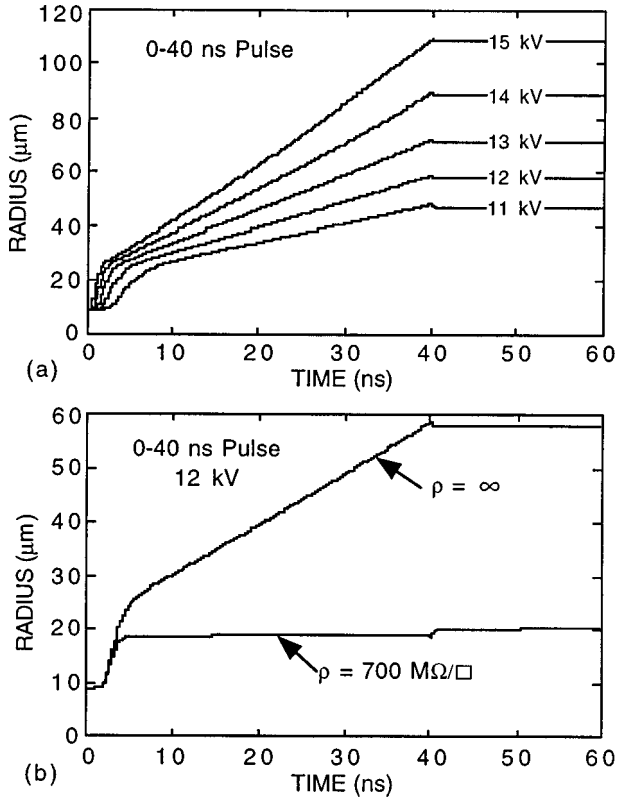

FIG. 2. Radius of the microdischarge in N_2 as a function of (a) line voltage and (b) with/without surface conductivity. In the absence of a mechanism to reduce gap voltage ahead of the body of the microdischarge, the microdischarge continues of expand as long as voltage is applied. A small surface conductivity bleeds charge to larger radii, thereby reducing the gap voltage and halting expansion.

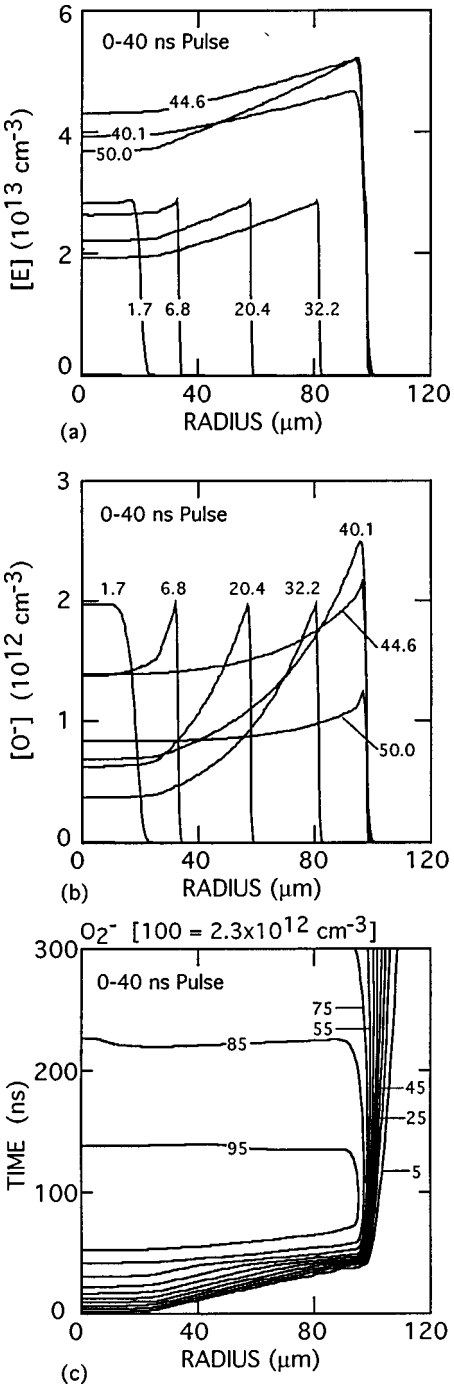

FIG. 3. Charged particle densities for a microdischarge in $N_2/O_2 = 80/20$. (a) Electron density, (b) O^- density and (c) O_2^- density. A moderate amount of attachment at intermediate values of E/N reduces the electron density in the core of the microdischarge. The labeling scheme is the same as in Fig. 1.

sitively on the line voltage. In agreement with Eliasson and Kogelschatz,[3] we found that the rate of microdischarge expansion is largely a function of the rate of electron avalanche, which for our conditions increases with increasing voltage. This trend is shown in Fig. 2(a) where the microdischarge radius is plotted a function of time for increasing charging voltage during a 40 ns pulse. The microdischarge radius increases nearly linearly with time after the first 5–10 ns. The short induction time is the duration required for electron avalanche to increase the axial current to the magnitude required to fully charge the dielectric. At that time, gap voltage collapses in the center of the microdischarge. This induction time decreases with increasing line voltage.

In the absence of there being a mechanism to charge the dielectric at larger radii than the expanding microdischarge, a process which removes voltage from the gap, the microdischarge will continue to grow as long as the voltage is applied as we have shown here. (Under conditions of high energy deposition hydrodynamic effects which rarefy the microdischarge core and ''snow plow'' a high gas density shell will reduce the E/N at large radius and eventually terminate expansion.[17] The energy deposition in all cases discussed here is insufficient for this to occur.) The experimental observation is that the expansion of the microdischarge stalls after 10–30 ns. In the two-dimensional modeling results of Eliasson and Kogelschatz, in which the electric potential is obtained from solving Poisson's equation in the (r,z) plane, charging of the dielectric produced a lateral component of the electric field.[3] This lateral component redirected charge flowing to the dielectric to radii greater than the main body of the microdischarge. The reduced gap voltage at large radii (or lengthened field lines) lowered ionization rates sufficiently to stall expansion. In our one-dimensional model, we can capture this behavior by allowing a finite surface conductivity (or less than infinite surface resistance) for the dielectric. The finite surface resistance allows the charge on the dielectric to spread laterally to larger radii than the microdis-

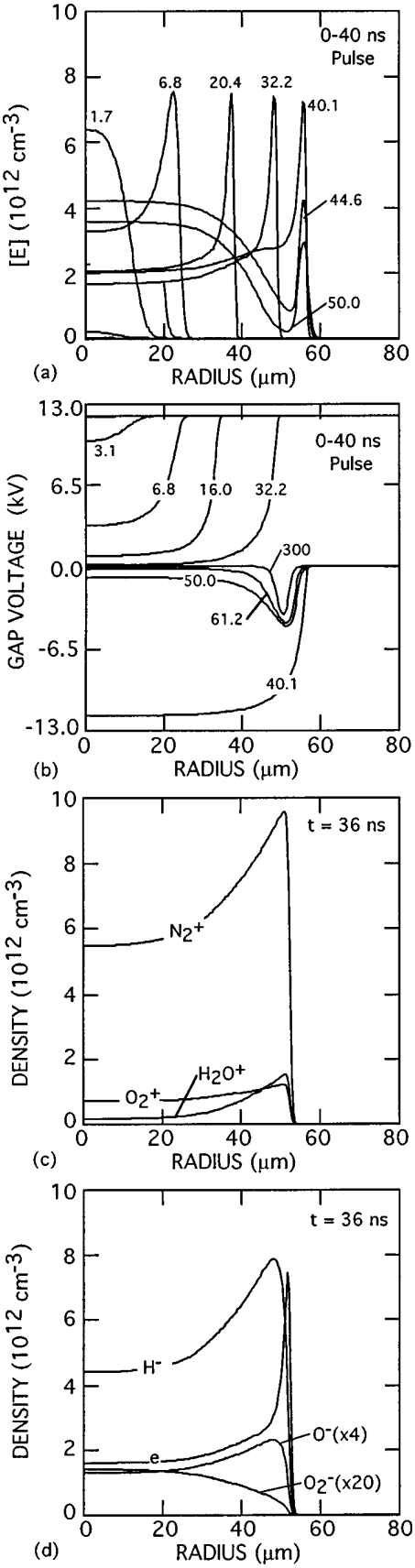

FIG. 4. Microdischarge parameters for an $N_2/O_2/H_2O=80/5/15$ plasma. (a) Electron density, (b) gap voltage, (c) positive ion densities at 36 ns and (d) negative ion densities at 36 ns. The larger rate of attachment and momentum transfer at intermediate E/N depletes the electron density in the core of the microdischarge as the dielectric charges. The labeling scheme is the same as in Fig. 1.

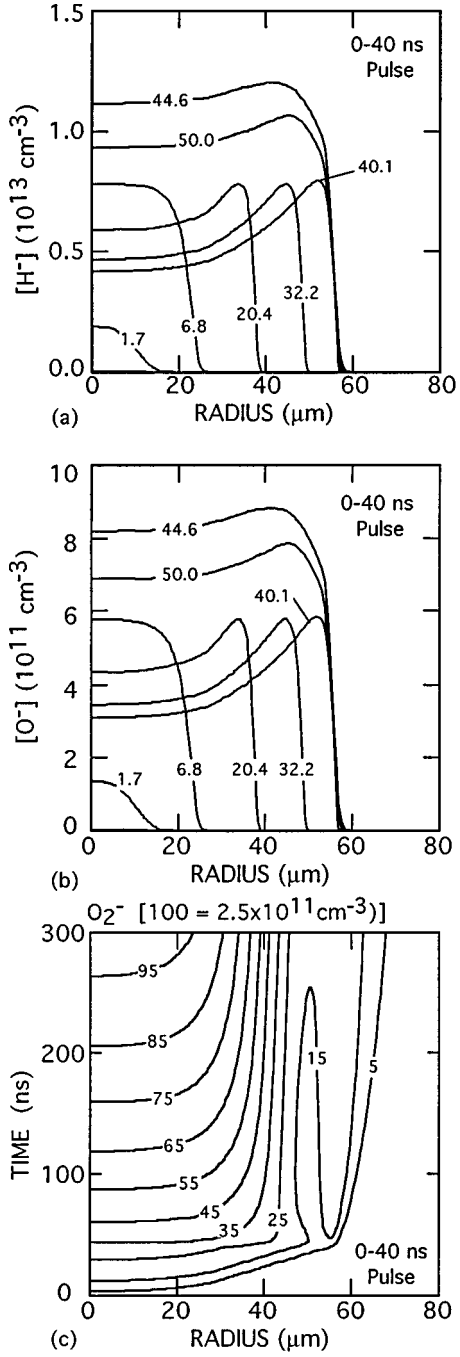

FIG. 5. Negative ion densities in a microdischarge sustained in $N_2/O_2/H_2O=80/5/15$. (a) H^-, (b) O^-, and (c) O_2^-. The negative ion densities persist in the core to long times, particularly near the edge of the microdischarge where the electrons are depleted by attachment. The labeling scheme is the same as in Fig. 1.

charge region. As a result, the gap voltage at large radii is eventually reduced to values lower than that required for avalanche. This reduction in gap voltage stalls the expansion of the microdischarge during the voltage pulse. For example, the microdischarge radius is shown in Fig. 2(b) as a function of time for a 12 kV pulse with and without surface conductivity. The expansion of the microdischarges is similar in the initial stage ($<4-5$ ns). Lateral charging of the dielectric when there is a non-zero surface conductivity, however, essentially halts the expansion after ≈ 5 ns. Further expansion

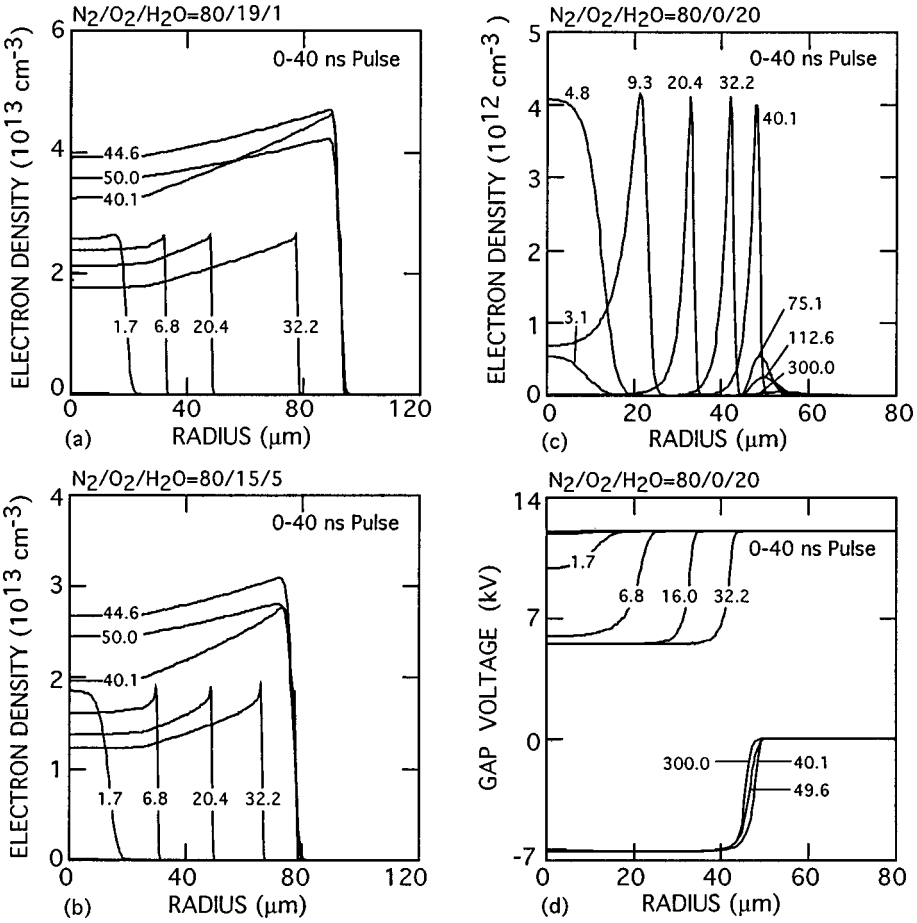

FIG. 6. Microdischarge characteristics for $N_2/O_2/H_2O$ mixtures with increasing mole fractions of water. The electron density as a function of radius at increasing times during the microdischarge are shown for $N_2/O_2/H_2O$=(a) 80/19/1, (b) 80/15/5, (c) 80/0/20. The gap voltage is shown in (d) for the 80/0/20 mixture. With increasing water mole fraction, the electron density is depleted by attachment more rapidly, leaving a shell of electron density. The electron current density is eventually small enough that the dielectric is not fully charged. The curves are labeled by their times (ns) after the application of the voltage pulse.

is slow although there is some small amount of additional microdischarge growth during the secondary avalanche. In the case of there being no surface conductivity, the microdischarge expands as long as there is voltage across the gap.

In the remainder of this article, we will discuss microdischarges generated by a 40 ns voltage pulse without surface conductivity for the dielectric and so produce a microdischarge which expands as long as there is applied voltage. These conditions are most conducive to isolating and investigating changes in charged particle composition resulting from dielectric charging. By doing so we ignore changes in the surface conductivity of the dielectric, which ultimately determine the maximum radius of the microdischarge, which may be caused by, for example, adding water to an otherwise dry gas mixture. We have found in side by side comparisons that the computed ion densities, particularly in the core of the microdischarge, are essentially the same whether we include or exclude surface conductivity up to the time at which the expansion stalls. The results which follow can be applied to specific cases of known microdischarge duration on that basis.

Negative ion and electron densities for a microdischarge through dry air (N_2/O_2=80/20) for the standard conditions are shown in Fig. 3 during and after the 40 ns voltage pulse. In comparison to pure nitrogen, the dry air discharge expands faster, a consequence of the larger rate of avalanche for a given E/N. The peak electron density during the primary avalanche is $\approx 3\times 10^{12}$ cm^{-3}, somewhat higher than that for N_2. The primary source of O^- is dissociative attachment to O_2, whose rate coefficient increases with increasing E/N over the range of interest. The primary sink for O^- is ion-ion neutralization whose rate coefficient at atmospheric pressure is $\approx 2\times 10^{-6}$ cm^{-3} s^{-1}. We therefore see a sharp rise in the O^- density at the leading edge of the expanding microdischarge where the rate coefficient for its formation is largest, and a decrease in the O^- density at trailing edge and center of the microdischarge where the E/N and dissociative attachment rates are smaller. Additional sinks of O^-, such as $O^- + O \rightarrow O_2 + e$, also contribute to reducing the O^- density in the center of the microdischarge. The electron density also decreases in the center of the microdischarge, though at a lower rate due to its lower rate of electron-ion recombination and due to there being a source of electrons from O^- detachment. The density of O_2^- does not exhibit a peak at the leading edge of the expanding microdischarge since the rate coefficient for three-body attachment decreases with increasing E/N and will, in fact, increase after the voltage collapses in the gap.

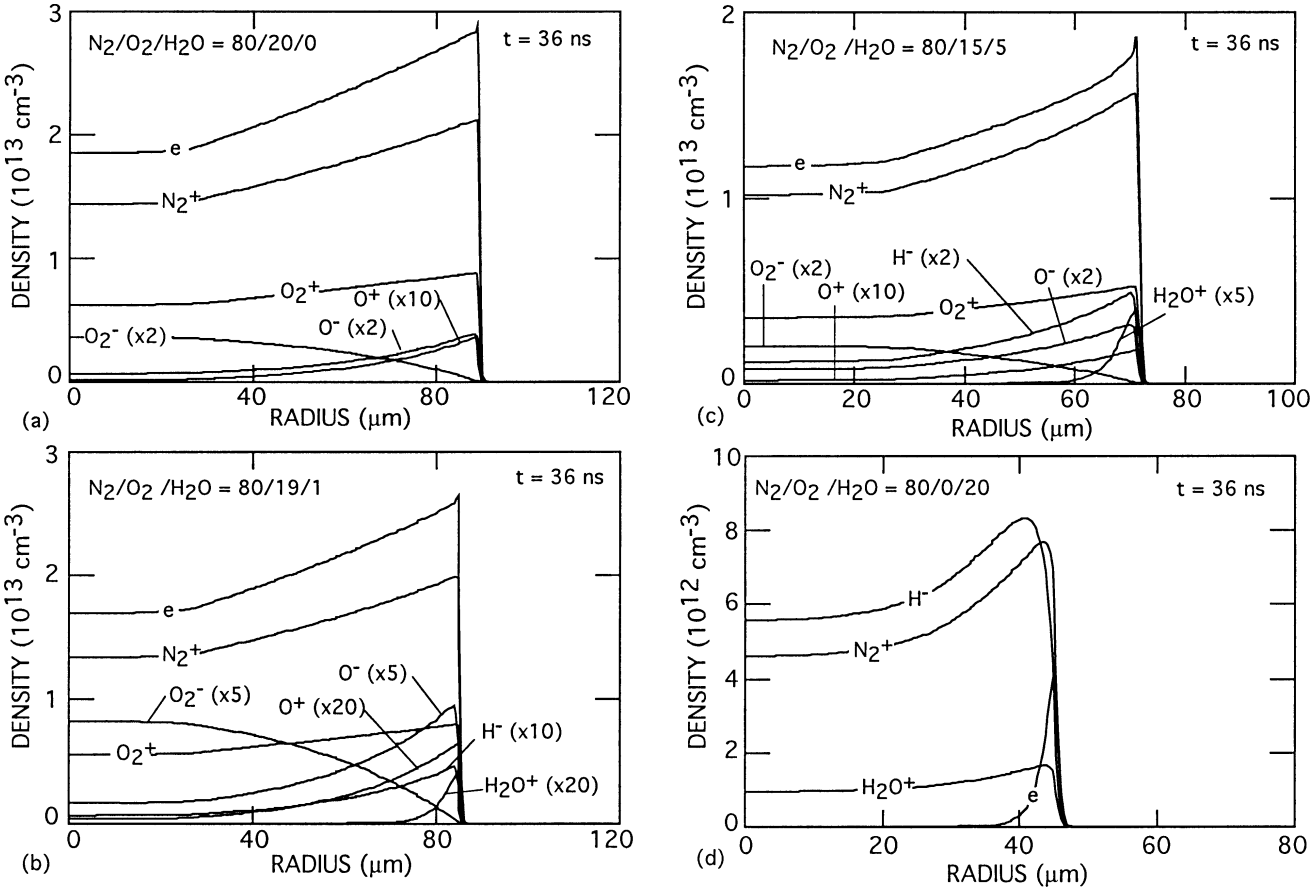

FIG. 7. Ion densities at 36 ns for microdischarges in $N_2/O_2/H_2O$=(a) 80/20/0, (b) 80/19/1, 80/15/5 and 80/0/20. The core of the microdischarge is essentially a negative ion-positive ion plasma with the higher water mole fraction.

The microdischarge dynamics of $N_2/O_2/H_2O$ mixtures differs markedly from that of dry air. For example, the electron density and gap voltage are shown in Fig. 4 for a $N_2/O_2/H_2O$=80/5/15 mixture, as might be found in combustion effluent. Ion densities at 36 ns are also shown. Negative ion densities as a function of time (H^-, O^-, O_2^-) are shown in Fig. 5. During the 40 ns voltage pulse, the electron density sharply peaks at the edge of the microdischarge, a much more dramatic effect than in dry air. The peak electron density is lower than either the nitrogen or dry air cases due to the higher rate of momentum transfer and attachment to H_2O. A major consequence of adding H_2O (and decreasing O_2) is that the rate of electron attachment at intermediate E/N (below avalanche) increases and the rate of detachment of O^- decreases. The end result is that as the dielectric charges and voltage collapses in the center of the microdischarge, the attachment rate increases and the electron density decreases. The lower electron current density in the center of the microdischarge is, in fact, sufficiently small that the dielectric does not totally charge to the line voltage, as shown in Fig. 4(b). That is, a residual voltage remains across the gap, and particularly so at large radius compared to the case for nitrogen or dry air. The electron density has a strong maximum near the edge of the microdischarge while the negative ion densities are more uniform in comparison. The hollow core of the electron density profile results from rapid losses to attachment, followed by slower rates of loss of the negative ions. The positive ion densities [Figs. 4(c) and 4(d)], which are largely immune to these dynamics, do not show the sharp peaking at large radius as does the electron density.

When the 40 ns voltage pulse terminates and the line voltage is driven to zero, the ''reverse voltage'' resulting from the dielectric charging [time 40.1 ns in Fig. 4(b)] produces a secondary avalanche near the center of the microdischarge. The secondary avalanche eventually fully discharges the dielectric. However, at large radii, the reverse voltage is sufficiently low, due to incomplete dielectric charging, that avalanche does not occur. In fact, the low E/N at that radius merely serves to increase attachment to O_2 and H_2O, which further reduces the electron density, as shown in Fig. 4(a). The end result is a residual charge on the dielectric which persists to long times. Any surviving residual voltage will then add to the applied voltage on the negative half of the voltage cycle.

The maximum electron density generally decreases with increasing water content. For example, electron densities for $N_2/O_2/H_2O$=80/19/1, 80/15/5 and 80/0/20 are shown in Fig. 6, as is the gap voltage for the latter case. Positive ion densities at 36 ns, and negative ion densities for the 80/0/20 case, are shown in Fig. 7. As the water content increases, the ''hollow shell'' appearance of the electron density increases, and dramatically so for the $N_2/O_2/H_2O$=80/0/20 mixture. Due to the large fraction of H_2O, the attachment rate is larger at all E/N, and the self sustaining E/N is higher, compared to

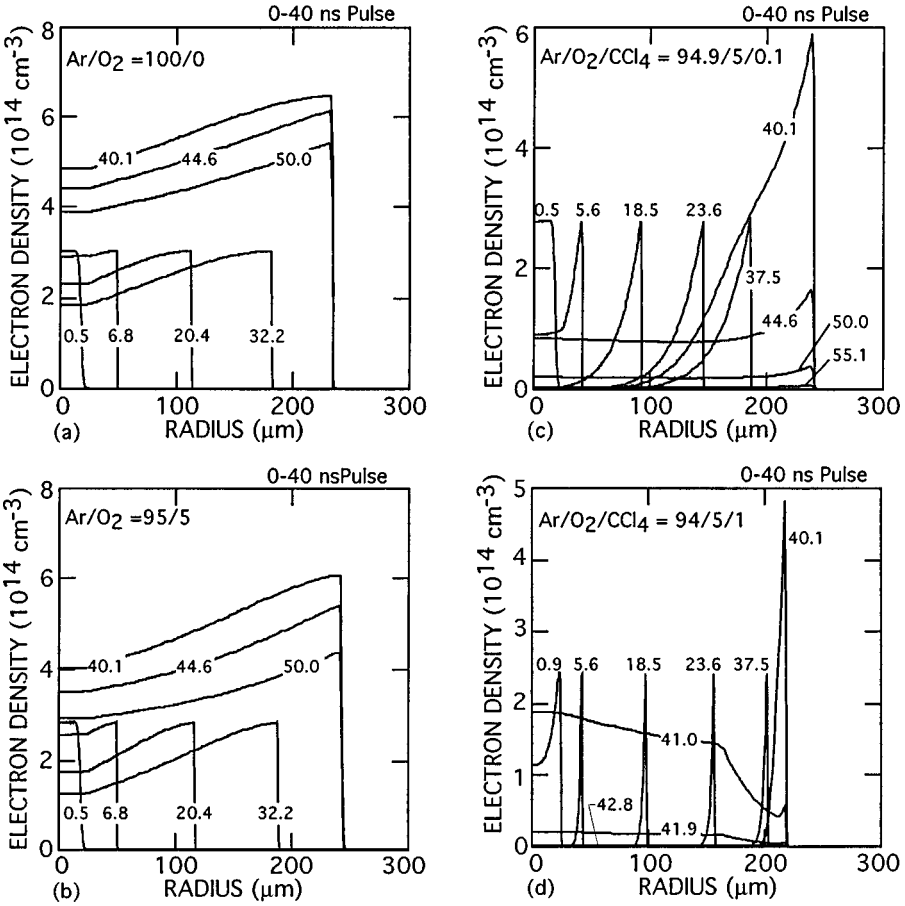

FIG. 8. Electron densities as a function of radius at increasing times for microdischarges in $Ar/O_2/CCl_4$. (a) 100/0/0, (b) 95/5/0, 94.9/5/0.1 and 94/5/1. As the CCl_4 density increases, the ''shell'' of expanding electron density becomes thinner. The electron density in the core of the microdischarge for the larger CCl_4 density is below 10^8 cm^{-3}. The curves are labeled by their times (ns) after application of the voltage pulse.

N_2/O_2 mixtures. At the leading edge of the voltage pulse, avalanche ramps the electron density to a peak of $\approx 4 \times 10^{12}$ cm^{-3}. As the dielectric charges and removes voltage from the gap in the center of the microdischarge, attachment soon dominates, driving the electron density to low values ($\approx 10^{10}$ cm^{-3}). The rapid decrease in electron density at small radii leaves an expanding shell of avalanching electrons and an inner core which is essentially a negative ion-positive ion plasma, as shown in Fig. 7.

The low electron density in the core for the $N_2/O_2/H_2O = 80/0/20$ case reduces the current density to a sufficiently low value that the dielectric again cannot fully charge. This leaves ≈ 6.5 kV across the gap. When the pulse is terminated and the line voltage is driven to zero, the small residual dielectric charge generates an insufficient voltage to produce a secondary avalanche. As a result, the dielectric charge persists and will be available to add to the negative potential applied on the second half of the voltage cycle.

The transition of the core of the microdischarge from an electron-positive ion plasma to a negative ion-positive ion plasma is seen in the sequence of plots in Fig. 7. At low water content, attachment is insufficient to completely quench the electron density. The negative charge density in the core of the microdischarge is dominated by electrons, and the dielectric fully charges to the line voltage. With increasing water content, attachment rates at low E/N increase, and there is a rapid transition to a negative ion-positive ion plasma following the avalanche wave. Charging of the dielectric is incomplete.

Plasma remediation of VOCs is typically performed in closed cycle systems to both contain products and to tailor the gas mixture for optimum efficiency. For example, mixtures of $Ar/O_2/H_2O/VOC$ or $Ar/O_2/VOC$ have been investigated for remediation.[8] CCl_4 is a particularly interesting VOC in this regard due to its large rates of dissociative electron attachment at low E/N.[20] As a result, the spatial distribution of the electron density can be heavily influenced by even small admixtures of CCl_4.

For comparison, the electron densities during microdischarge development in $Ar/O_2/CCl_4 = 100/0/0$, 95/5/0, 94.9/5/0.1 and 94/5/1 gas mixtures are shown in Fig. 8. Selected ion densities at 36 ns are shown in Fig. 9. The qualitative behavior of the Ar microdischarge is similar to that of the N_2 discharge. The microdischarge expands radially, fully charging the dielectric leaving behind a positive ion-electron plasma which slowly recombines. A secondary discharge raises the electron and ion density across the entire ''preionized'' radius when the line voltage is pulled to zero. The addition of 5% O_2 does not appreciably change the electron profiles other than reducing the density in the low E/N core due to attachment. However, with addition of 0.1% CCl_4 ($Ar/O_2/CCl_4 = 94.9/5/0.1$) there is a large increase in the at-

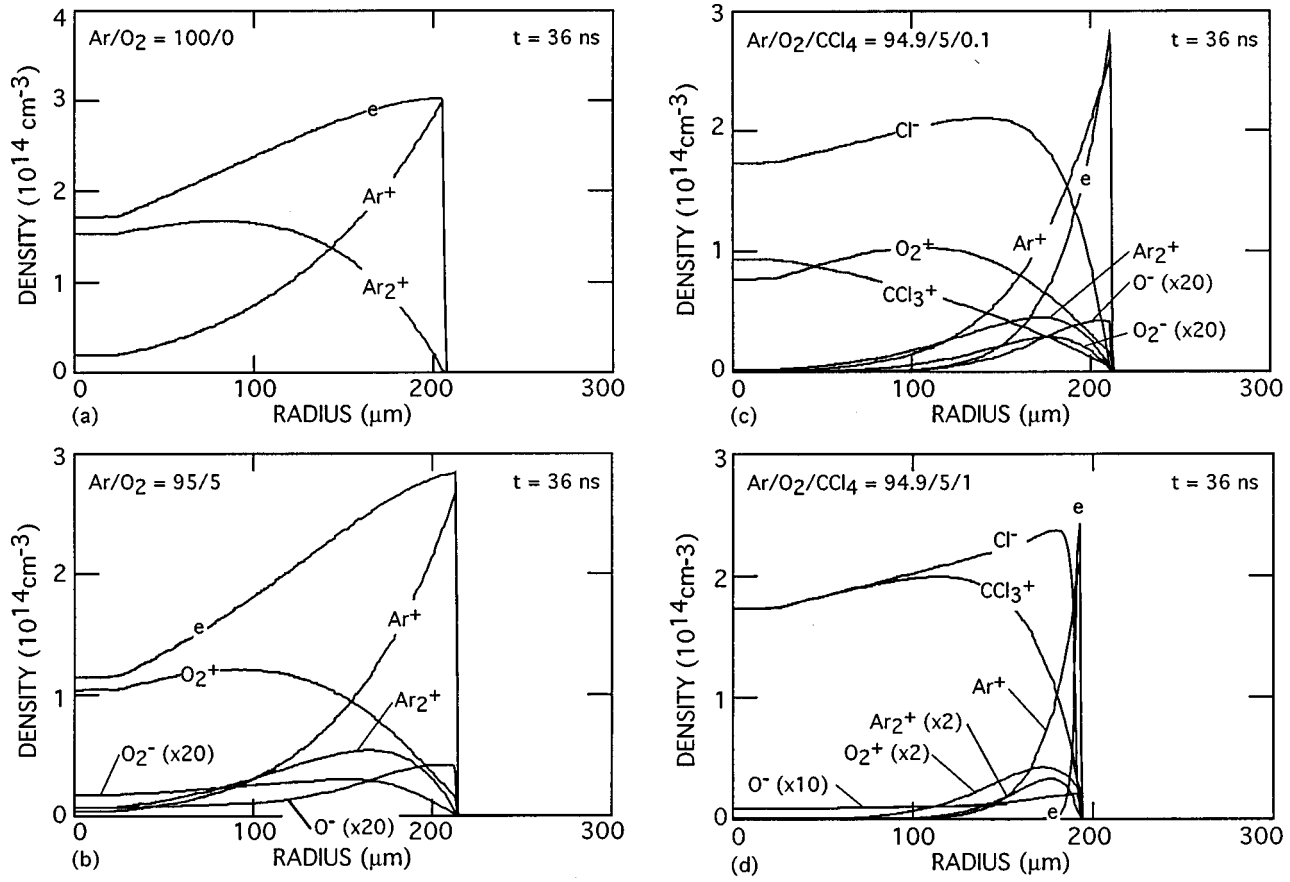

FIG. 9. Ion densities as a function of radius at 36 ns for microdischarges in $Ar/O_2/CCl_4$. (a) 100/0/0, (b) 95/5/0, 94.9/5/0.1 and 94/5/1. As the CCl_4 density increases, the core of the microdischarge progresses from an electron-positive ion plasma to a negative ion-positive ion plasma.

tachment rate at low E/N. As the dielectric charges, thereby lowering E/N in the center of the microdischarge, attachment dominates leaving behind an expanding avalanching shell of electrons, and a core which is largely composed of negative ions and positive ions. This effect is heightened by increasing the CCl_4 fraction to 1% ($Ar/O_2/CCl_4 = 94/5/1$). Here the higher attachment rate in the core consumes the electrons within a few ns of the local E/N falling below a self-sustaining value, leaving behind a thin electron shell. The charged particle core of the microdischarge is composed almost exclusively of CCl_3^+ and Cl^-. Other positive ions on the leeward side of the electron shell undergo charge exchange, ultimately producing CCl_3^+. The dielectric does not fully charge, but there is sufficient voltage for a short secondary avalanche. The secondary avalanche generates more uniform electron distribution within the streamer due to ''preionization.''

IV. CONCLUDING REMARKS

Microdischarge dynamics in dielectric barrier discharges have been investigated for gas mixtures with varying degrees of electronegativity. We found that in electropositive mixtures, the expanding microdischarge retains a fairly uniform electron density as a function of radius, suffering a small reduction in the core of the microdischarge due to electron-ion recombination. Dielectric charging and the reduction of E/N at small radius has little effect on recombination rates. However, in electronegative gas mixtures, particularly those whose attachment rates increase with decreasing E/N, the core of the microdischarge may quickly evolve to a negative ion-positive ion plasma. This effect is particularly acute in thermal attaching gas mixtures such as those containing CCl_4. Microdischarge expansion will, in the absence of dielectric charging at radii ahead of the core, proceed unimpeded as long as voltage is available. The stalling of the expansion is attributed to transverse components of the electric field on or near the dielectric which charges the dielectric ahead of the body of the microdischarge.

ACKNOWLEDGMENTS

This work was supported by the National Science Foundation (CTS 94-12565) and the Office of Naval Research (N00014-94-1-0819).

[1] H. Bertein, J. Phys. D: Appl. Phys. **6**, 1910 (1973).
[2] B. Eliasson, M. Hirth, and U. Kogelschatz, J. Phys. D: Appl. Phys. **20**, 1421 (1987).
[3] B. Eliasson and U. Kogelschatz, IEEE Trans. Plasma Sci. **19**, 309 (1991).
[4] W. Sun, B. Pashaie, and F. Honea, J. Appl. Phys. **79**, 3438 (1996)
[5] A. C. Gentile and M. J. Kushner, J. Appl. Phys. **78**, 2074 (1995).
[6] B. M. Penetrante, M. C. Hsiao, B. T. Merritt, and G. E. Vogtlin, Appl. Phys. Lett. **66**, 3096 (1995).
[7] W. Sun, B. Pashaie, S. K. Dhali, and F. I. Honea, J. Appl. Phys. **79**, 3438 (1996).
[8] L. A. Rosocha, G. K. Anderson, L. A. Bechtold, J. J. Coogan, H. G. Heck, M. Kang, W. H. McCulla, R. A. Tennant, and P. J. Wantuck, in *Nonther-*

mal Plasma Techniques for Pollution Control, Part b, edited by B. M. Penetrante and S. E. Schultheis (Springer, Berlin, 1993), p. 281.
[9] D. Evans, L. A. Rosocha, G. K. Anderson, J. J. Coogan, and M. J. Kushner, J. Appl. Phys. **74**, 5378 (1993).
[10] M. B. Chang and C. C. Lee, Environ. Sci. Technol. **29**, 181 (1995).
[11] M. C. Hsiao, B. T. Merritt, B. M. Penetrante, and G. E. Voglin, J. Appl. Phys. **78**, 3451 (1995).
[12] R. G. Tonkn, S. E. Barlow, and T. M. Orlando, J. Appl. Phys. **79**, 3451 (1996).
[13] Z. Falkenstein, J. Adv. Oxid. Technol. **1**, 223 (1997).
[14] D. Braun, U. Kuchler, and G. Pietsch, J. Phys. D: Mem. **24**, 564 (1991).
[15] Z. Falkenstein and J. Coogan, J. Phys. D: Appl. Phys. **30**, 817 (1997).
[16] D. Braun, V. Gibalov, and G. Pietsch, Plasma Sources Sci. Technol. **1**, 166 (1992).
[17] A. C. Gentile and M. J. Kushner, J. Appl. Phys. **78**, 2977 (1995).
[18] P. A. Thompson, *Compressible Fluid Dynamics* (McGraw–Hill, New York, 1972), Appendix E.
[19] J. O. Hirschfelder, C. F. Curtiss, and R. B. Bird, in *Molecular Theory of Gases and Liquids* (Wiley, New York, 1954), Chap. 8.
[20] L. Bromberg, D. R. Cohn, M. Koch, R. M. Patrick, and P. Thomas, Phys. Lett. A **173**, 293 (1993).